Mars Odyssey Accelerometer: Report on Data Processing, Archiving, and Analysis

Paul Withers[a,*]

[a] Center for Space Physics, Boston University, 725 Commonwealth Avenue, Boston, MA 02215, USA.

[*] Corresponding author email address: withers@bu.edu

Number of pages: 28

Number of figures: 1

Number of tables: 4

Proposed Running Head:

Odyssey Accelerometer Data

Editorial Correspondence to:

Paul Withers

Center for Space Physics, Boston University,

725 Commonwealth Avenue, Boston, MA 02215, USA.

Email: withers@bu.edu

Phone: (617) 353 1531

Fax: (617) 353 6463

Received _____; accepted _____

Formatted using AASTEX aasms4.sty

ABSTRACT

This is a rough draft of a work in progress. Once completed, this manuscript will serve two purposes. First, source material for PDS documentation describing the generation of these data products. Second, source material for a scientific paper that briefly describes the generation of these data products and spends more time describing some analysis and interpretation of these data products. It accompanies a set of data products placed on my website so that users of the data products can understand how they were generated.

Keywords: Mars, Atmosphere; Data Reduction Techniques

1. Introduction

This paper describes the processing of Mars Odyssey accelerometer data and the results of preliminary scientific analysis of the derived data products.

The Mars Odyssey accelerometer (ACC) instrument was used to measure atmospheric densities during aerobraking. These measurements influenced operational decisions during aerobraking, such as changes to periapsis altitude. The instrument was not part of the mission's scientific payload and its data were not archived at the Planetary Data System (PDS) in the usual manner. We have acquired ACC data and derived measurements of Mars atmospheric properties from them. This paper describes the ACC dataset, describes how it was processed, and presents some scientific interpretation of its measurements.

2. Accelerometer Instrument and Available Data

Odyssey's ACC instrument consisted of two inertial measurement units (IMUs). Each IMU contained three single-axis accelerometers, each of which measured linear acceleration along the accelerometer's axis at the position of the relevant sensor, and three single-axis gyroscopes, each of which measured angular velocity along the gyroscope's axis at the position of the relevant sensor. These measurements were converted into three-axis linear acceleration and three-axis angular velocity at a single position within the IMU before being transferred out of the IMU. "The primary IMU was used throughout aerobraking. The internal orientation of two of the three [single-axis] accelerometers was not aligned with the body axes, and so data from these two accelerometers were combined in the ground data system to form body axes accelerations." REF to Tolson JSR quotation.

In this work, we concentrate exclusively on the three-axis linear acceleration measurements and do not use the three-axis gyroscope measurements. Odyssey produced

two distinct data streams of three-axis acceleration measurements, low rate and high rate, both of which have a nominal interval between measurements of 1 second. The generation of the high rate data stream was reported in (REF Tolson JSR). Odyssey's onboard computer sampled the IMU's output 200 times per second. For orbits 1–136, the average of every 200 samples was sent to the high rate data stream. For orbits 137–268, the average of the first 50 of every 200 samples was sent to the high rate data stream. For orbits 269–336, the average of the first 20 of every 200 samples was sent to the high rate data stream (Tolson). Onboard memory limitations and the increase in the duration of aerobraking passes as the mission progressed were responsible for this steady degradation in data quality. The generation of the low rate data stream has not been discussed in the scientific literature. Its noise characteristics do not change during aerobraking, which suggests that the same sampling rate was used throughout aerobraking. Based on comparisons to the high rate data stream, the noise characteristics of the low rate data stream are consistent with the low rate data stream containing one of the 200 samples collected every second, rather than containing the mean of a subset of those 200 samples.

Low rate data have been delivered to the PDS Atmospheres Node in a non-standard format, but have not yet been peer-reviewed nor accepted into the PDS. Acceleration measurements for each orbit were provided in an ASCII file (pXXXacc.txt) that contains time in YY/DOY-HH:MM:SS.SSS format and x, y, and z-axis accelerations in m s^{-2}. There is no accompanying documentation. Many time standards are used by spacecraft missions (REF). These times were confirmed to be UTC times, not barycentric dynamical times or ephemeris times (ET), by reproduction of Tolson et al.'s plots of acceleration/density versus time since periapsis for P076 (REF Tolson). We assumed that the x, y, and z-axes were those of the "M01_SPACECRAFT" frame defined by SPICE kernel m01_v28.tf, which is identical to the Lockheed Martin (LMA) mechanical coordinate system for Odyssey (REFS to SPICE and Takashima).

High rate data have been delivered to the PDS Atmospheres Node in a non-standard format, but have not yet been peer-reviewed nor accepted into the PDS. Acceleration measurements for each orbit were provided in a MATLAB file (LOPXXX.mat). Some documentation was provided in Microsoft Excel and Word files. We extracted variables HiACCTime and HiACC from each orbit's LOPXXX.mat file. According to the documentation, HiACCTime is time expressed as UTC seconds past J2000. These were confirmed to be UTC seconds, not ET seconds, by reproduction of Tolson et al.'s plots of acceleration/density versus time since periapsis for P076 (REF Tolson). According to the documentation, HiACC is x, y, and z-axis accelerations in m s^{-2}. These accelerations are similar to the low-rate accelerations, which suggests that they are expressed in the same coordinate system. Therefore we again assumed that the x, y, and z-axes were those of the "M01_SPACECRAFT" frame defined by SPICE kernel m01_v28.tf, which is identical to the Lockheed Martin (LMA) mechanical coordinate system for Odyssey (REFS to SPICE and Takashima).

We extracted the low rate and high rate data from these files, then discarded some isolated data points. High rate data for hundreds of orbits contain gaps of >30s towards the end of the outbound leg. Data after these gaps were discarded. There is an additional gap of >5s towards the end of the outbound leg in high rate data for both P109 and P173. Data after these gaps were discarded. There is a gap of 3s between the last and penultimate data points in orbits 26, 27, 28, 38, 69, 74, 123, 155, 170, 179-189, 249, 273, 276, 285, 292, 297, 299, 301, 303, 305, and 306. The last data point was discarded in these orbits. Gaps of 1s-2s in the high rate data remain in about 20% of the orbits. These are short enough that their effects are minimal, so the data were not modified to correct for them. This completes step 1 (data cleaning) of the data processing.

No data exist for orbits 1, 2, 3, 5, and 327. "Quick Look Reports" that summarized

ACC measurements from a given aerobraking pass were generated by the ACC team in support of mission operations for each orbit when Odyssey was aerobraking. No "Quick Look Reports" were generated for these orbits, which suggests that no useful data were received on the ground, not that a file was accidently omitted from those delivered to the PDS. Low rate data, but not high rate data, exist for orbits 4, 57, 158, 213, 255, 266, 289, and 336. The high rate data stream for orbit 137 begins well inside the atmosphere, close to periapsis, and contains measurements at 4 s intervals instead of the usual 1 s intervals. The low rate data for orbit 137 are normal. Data for orbits 4 (low rate only, periapsis altitude = 290 km) and 6 (low rate and high rate, periapsis altitude = 160 km) exist, but aerodynamic accelerations cannot be separated from non-aerodynamic accelerations when altitudes are so high and aerodynamic drag is so weak (see Section XXX). Results for orbits 1-336 used the following data streams. No results for orbits 1, 2, 3, 4, 5, 6, 327. Results based on low rate data for orbits 57, 137, 158, 213, 255, 266, 289, and 336. Results based on high rate data for all other orbits.

FIGURE - Any figures of rawish data?

3. Spacecraft Position, Velocity, and Orientation

The position, velocity, and orientation of Odyssey in an inertial reference frame during aerobraking were obtained from SPICE kernels m01_ab.bsp, m01_sc_ab0110.bc, m01_sc_ab0111.bc, m01_sc_ab0112.bc, m01_sc_ab0201.bc, and m01_sc_ab0202.bc (REF). The position and orientation of Mars in an inertial reference frame were obtained from SPICE kernels de414.bsp and pck00008.tpc. Time-related SPICE kernels naif0008.tls and orb1_sclkscet_00129.tsc were also used in this work. The velocity of the Mars atmosphere, assuming that it rotates with the solid body of the planet, in an inertial reference frame was calculated using these SPICE kernels. The velocity of the atmosphere relative to the

spacecraft and of the spacecraft relative to the atmosphere can be determined from this information. Spacecraft altitude was defined as $\left|\underline{r_{ODY}} - \underline{r_A}\right|$, where $\underline{r_{ODY}}$ is the position of the spacecraft relative to the centre of mass of Mars, $\underline{r_A}$ is the position of a point on the Mars areoid relative to the centre of mass of Mars, and $\underline{r_{ODY}}$ is parallel to $\underline{r_A}$. The MOLA 0.25 x 0.25 degree areoid was used (REF mega90n000cb.img). Periapsis is defined in this paper as the point of minimum altitude, not minimum radial distance.

SPICE kernels for Odyssey's orientation are not available on 28 November 2001, which encompasses aerobraking passes on orbits 58 and 59. Odyssey's attitude on these orbits was assumed to be $\phi = 0°$ and $\theta = -4°$, where ϕ and θ are defined in Section 7 (REF TOLSON 2005). This attitude, the nominal trim attitude, is consistent with Odyssey's average attitude for neighbouring orbits.

FIGURES - Periapsis z, lat, LST, Ls, anything else vs orbit number.

4. Acceleration Corrections

We wish to derive atmospheric densities, ρ, from aerodynamic accelerations, $\underline{a_{aero}}$. Measured accelerations, $\underline{a_{meas}}$, are not identical to $\underline{a_{aero}}$. They are related by:

$$\underline{a_{meas}} = \underline{a_{bias}} + \underline{a_{aero}} + \underline{a_{gg}} + \underline{a_{thr}} + \underline{\omega} \times (\underline{\omega} \times \underline{r}) + \underline{\dot{\omega}} \times \underline{r} \tag{1}$$

Push a lot of this to an Appendix if published

$\underline{a_{bias}}$ represents the effect of sensor bias, $\underline{a_{gg}}$, which is called the gravity gradient term, represents the effect of differences between the acceleration due to gravity at the sensor and at the spacecraft's centre of mass, $\underline{a_{thr}}$ represents the effect of reaction control system (RCS) thruster firings, ω is the angular velocity of the spacecraft, $\underline{r}$ is the position of

the accelerometer with respect to the spacecraft's centre of mass, an overdot indicates a derivative with respect to time, and the last two terms represent the effects of angular motion of the sensor about the spacecraft's centre of mass. The derivation of atmospheric densities uses only the y-axis component of $\underline{a_{aero}}$, so we focus on the y-axis component of Eqn 1. We now address each term in Eqn 1.

The two angular acceleration terms can, in principle, be calculated. SPICE orientation information is sufficient to determine $\underline{\omega}$ and $\underline{\dot{\omega}}$. However, we do not know $\underline{r}$ accurately. The positions of the accelerometer and the centre of mass were measured before launch. The accelerometer has not moved since then, but the centre of mass has. Fuel consumption causes a secular change in centre of mass position. Accelerations experienced during aerobraking cause the fuel to slosh back and forth in the tanks, which also alters centre of mass position. Rapid changes in $\underline{r}$ could introduce an additional term, a Coriolis term, into Eqn 1. According to Tolson et al., the accelerometer position is (x,y,z) = (0.164, -0.544, 1.137) metres relative to the centre of mass. However, the reference frame for this position is not defined. The spacecraft axes defined by Tolson et al.'s Figure 3 differ from "M01_SPACECRAFT" frame defined by SPICE. According to Chavis and Wilmoth, the accelerometer position at the midpoint of aerobraking was (x,y,z) = (-0.629, -00172, 1.1) metres relative to the centre of mass in the "body coordinate system." We do not correct $\underline{a_{meas}}$ for the two angular acceleration terms.

$\underline{a_{thr}}$ is "two orders of magnitude less than the periapsis drag effect" (Tolson). The typical acceleration at periapsis is 2×10^{-2} ms^{-2}, so the thruster term is on the order of 2×10^{-4} ms^{-2}. The nominal impulse, I, generated by a single RCS thruster firing is approximately $I = 0.00804038t + 0.0212576$, where t is the duration of the thruster firing in milliseconds and I is in N-sec (REF Nav small forces document). There are four RCS thrusters, labelled RCS1 to RCS4. The change in Odyssey's velocity due to an RCS thruster

firing, $\Delta\underline{v}$, equals $I\underline{\hat{e}}/m$ where m is Odyssey's mass and $\underline{\hat{e}}$ is a unit vector. $\underline{\hat{e}}_{RCS1}$ = (-X, Y, -Z), $\underline{\hat{e}}_{RCS2}$ = (-X, -Y, -Z), $\underline{\hat{e}}_{RCS3}$ = (X, -Y, -Z), $\underline{\hat{e}}_{RCS4}$ = (X, Y, -Z), where $X = 0.8926$, $Y = 0.4162$, and $Z = 0.1736$. These unit vectors are in the "M01_SPACECRAFT" frame. (REF NAV small forces again) Thruster firings are reported in ASCII files (pXXXthot.txt) that accompany the low rate accelerometer data. The cumulative times that each thruster has fired for are listed as functions of time. Typical thruster firings last for 0.1 sec, much less than the typical interval between cumulative times in pXXXthot.txt (1–10 sec). Since the times of thruster activity cannot be resolved, their contributions cannot be removed from the measured accelerations. Also, the actual impulse produced by a thruster will differ from the nominal impulse. Past experience has shown that determination of thruster impulse to within 50% is difficult (REF Tolson JSR). We do not correct $\underline{a_{meas}}$ for thruster activity.

$\underline{a_{gg}}$ is on the order of 1×10^{-6} ms^{-2} (Cancro). This is much smaller than $\underline{a_{thr}}$, so we neglect it.

When Odyssey is far outside the atmosphere, $\underline{a_{meas}} = \underline{a_{bias}}$. Pre-entry and post-exit measured accelerations can be used to estimate instrument bias. Scatter in $a_{meas,lo,y}$ (the y-component of the low rate measured acceleration) was large enough that estimates of $a_{bias,lo,y}$ could not be distinguished from zero. $a_{meas,lo,y}$ was not corrected for bias. $a_{bias,hi,y}$ was calculated from pre-entry and post-exit accelerations. The pre-entry value of $a_{bias,hi,y}$ was assumed to be the mean of all $a_{meas,hi,y}$ measurements from 10s after the start of the data stream to 60s later. The post-exit value of $a_{bias,hi,y}$ was assumed to be the mean of all $a_{meas,hi,y}$ measurements from 70s before the end of the data stream to 60s later. These time ranges were chosen to ensure that aerodynamic accelerations and any transients associated with the beginning/end of the data stream were negligible. The typical pre-entry bias was -2.4×10^{-4} ms^{-2} and the typical post-exit bias was -2.2×10^{-4} ms^{-2}. $a_{bias,hi,y}$ was

assumed to vary linearly with time during an aerobraking pass. The post-exit bias was assumed to equal the pre-entry bias for orbits 84, 91, 93, and 95 due to lack of adequate post-exit data. We correct $\underline{a_{meas}}$ for bias for high rate data only.

Thus $a_{aero,lo,y} = a_{meas,lo,y}$ and $a_{aero,hi,y} = a_{meas,hi,y}$ - $a_{bias,hi,y}$. This completes step 2 (data correction) of the data processing.

FIGURE - Plot of pre/post bias vs orbit number

FIGURE - amax, aero vs orbit number

5. Reducing Noise in the Data

Next, we formed 7-point and 39-point running means of $a_{aero,lo,y}$ and $a_{aero,hi,y}$, effectively 7-s and 39-s averages, and labelled them $a_{aero,lo,y,7}$, $a_{aero,lo,y,39}$, $a_{aero,hi,y,7}$, and $a_{aero,hi,y,39}$. This reduced the noise in the accelerations at the expense of spatial resolution. The duration of the 39-point time series is shorter than the duration of the 7-point time series, which is shorter than the duration of the unaveraged time series, because a 7-point running mean cannot be calculated for the first three data points in a series of measurements.

The noise inherent in $a_{aero,lo,y}$, $a_{aero,hi,y}$, $a_{aero,lo,y,7}$, $a_{aero,hi,y,7}$, $a_{aero,lo,y,39}$, and $a_{aero,hi,y,39}$ was estimated based on the standard deviation of selected pre-entry measurements. Measurements from 30s after the start of the time series to 60s later were used for $a_{aero,lo,y}$, $a_{aero,lo,y,7}$, and $a_{aero,lo,y,39}$. Measurements from 10s after the start of the time series to 200s later were used for $a_{aero,hi,y}$. Measurements from 10s after the start of the time series to 100s later were used for $a_{aero,hi,y,7}$. Measurements from 30s after the start of the time series to 60s later were used for $a_{aero,hi,y,39}$. The start times of these time series were chosen to ensure that transients associated with the beginning of the data stream did not affect any of the calculated noise values. The end times of these time series were chosen to ensure that

aerodynamic accelerations did not affect any of the calculated noise values. These time series were made as long as possible to increase the accuracy of the noise calculation.

Results are shown in Figure XXX and Table XXX; they do not conform to the expected $\sqrt{N}$ dependence for samples from a Gaussian distribution.

FIGURE - Plot of 1-sigma scatter vs orbit number, 7s, 39s

TABLE - Of what? Where do I pump these results out?

FIGURE - a vs t 1, 7, 39 for P076

6. Selection of Useful Data and Determination of Uncertainties

Useful data are data that are clearly dominated by aerodynamic acceleration, not other factors such as instrument noise (Figure XXX), the effects of thrusters, and the effects of angular accelerations (Section 4). We process the data to remove those that are not useful.

Accelerations due to thrusters are on the order of 2×10^{-4} ms^{-2} (Section 4). Let the magnitudes of the y-component of the two angular acceleration terms in Eqn 1 be Y_1 and Y_2 respectively. We estimate Y_1 and Y_2 using angular rate information from SPICE and $\underline{r} = (0.164, -0.544, 1.137)$ metres (REF Tolson JSR 2005, assumed to be in the M01_SPACECRAFT frame). Angular accelerations are greater with the value of $\underline{r}$ from Tolson et al. than from Chavis and Wilmoth, so this choice is conservative.

Data points that were smaller than a threshold were deemed to be not useful. The threshold was calculated for each time step and each of the six sets of accelerations ($a_{aero,lo,y}$, $a_{aero,lo,y,7}$, $a_{aero,lo,y,39}$, $a_{aero,hi,y}$, $a_{aero,hi,y,7}$, and $a_{aero,hi,y,39}$). The threshold was the largest of (A) the relevant noise level, (B) 2×10^{-4} ms^{-2}, (C) Y_1 and, (D) Y_2. The threshold was controlled by the effects of thrusters for $a_{aero,lo,y,7}$, $a_{aero,lo,y,39}$, $a_{aero,hi,y}$ (orbits 7–136),

$a_{aero,hi,y,7}$ and $a_{aero,hi,y,39}$, and by noise for $a_{aero,lo,y}$ and $a_{aero,hi,y}$ (orbits 137–336). Recall that the noise in the high rate data increased between orbits 136 and 137 (Section 2). Angular accelerations are not the limiting factor controlling the quality of Odyssey ACC data products.

Data points that were smaller than their corresponding threshold were discarded. This sometimes resulted in large gaps in the time series of retained data points, which is not desirable. To correct this, additional data points were discarded as necessary to ensure that the time series of retained data points was continuous. For example, if the data point at t=-50s exceeded its threshold, the data points from t=-49s to t=-40s did not exceed their threshold, and the data points from t=-39s to t=+60s exceeded their thresholds, the data point at t=-50s was discarded. Each retained data point was assigned an uncertainty equal to its corresponding threshold. This completes step 3 (data selection) of the data processing.

7. Derivation of Atmospheric Densities

The atmospheric density, ρ, satisfies:

$$m\,|a_{aero,y}| = \frac{\rho V^2 C_y A}{2} \tag{2}$$

where m is the spacecraft mass, $a_{aero,y}$ is the y-component of the aerodynamic acceleration, V is the scalar speed of the spacecraft relative to the atmosphere, or vice versa, C_y is an aerodynamic coefficient, and A is a reference area connected with C_y. Similar equations exist for all directions. We use the y-axis in the M01_SPACECRAFT frame since acceleration measurements along this axis, which is close to the velocity of the spacecraft relative to the atmosphere, have the greatest signal-to-noise ratio.

m varied from 460.8 kg at the start of aerobraking to 451.7 kg at the end (REF Reference to Bob Mase, show figure of m vs orbit number). Uncertainty in the absolute mass is 3 kg, although the change in mass from one orbit to the next orbit is known much more accurately. A is 11.03 m^2 (REF Jill Prince). V is known from SPICE information (Section 3). The product $\rho \times C_y$ can be found using measured or known quantities (m, $a_{aero,y}$, V, and A) at each time step along an aerobraking pass.

FIGURE - m vs orbit number

Next, ρ and C_y are determined from the product $\rho \times C_y$. Odyssey's C_y, typically $\sim$2, is a function of density and the attitude of the spacecraft with respect to its velocity relative to the atmosphere. Spacecraft attitude can be expressed as two angles, ϕ and θ. If the velocity of the atmosphere relative to the spacecraft is $\underline{U} = U\underline{u}$, where $\underline{u}$ is a unit vector expressed in the M01_SPACECRAFT frame, then pitch (ϕ) and yaw (θ) angles are defined by:

$$u_x = \cos\theta \sin\phi \tag{3}$$

$$u_y = \cos\theta \cos\phi \tag{4}$$

$$u_z = -\sin\theta \tag{5}$$

Values of C_y for various ρ, ϕ, and θ have been determined by numerical simulation. These values constitute the "aerodynamic database." Uncertainties in C_y are estimated to be 3% (REF?). Inputs to the numerical simulations ranged from 10^{-4} kg km^{-3} to 10^4 kg km^{-3} for ρ, from -60° to 60° for ϕ, and -60° to 60° for θ. These ranges encompassed all conditions encountered during aerobraking. The unit vector $\underline{u}$ was found as a function of time for each aerobraking pass (Section 3). Angles ϕ and θ were then determined using Eqns 3–5, also as functions of time for each aerobraking pass. At each time step in

each aerobraking pass, the simulated value of C_y was found as a function of ρ using the aerodynamic database. The simulated value of the product $\rho \times C_y$ was also found as a function of ρ.

$\rho \times C_y$ is a **single-valued function** of ρ for any specified ϕ and θ, which enables both ρ and C_y to be found from $\rho \times C_y$. At each time step in each aerobraking pass, the observed value of the product $\rho \times C_y$ and the simulated function $\rho C_y(\rho)$ were compared to determine the value of ρ and then C_y. This is illustrated in Figure X.

FIGURE - rho x Cy vs rho, also Cy vs rho for some nominal case, with nice words

This process was applied to $a_{aero,lo,y}$, $a_{aero,hi,y}$, $a_{aero,lo,y,7}$, $a_{aero,hi,y,7}$, $a_{aero,lo,y,39}$, and $a_{aero,hi,y,39}$ to obtain ρ_{lo}, ρ_{hi}, $\rho_{lo,7}$, $\rho_{hi,7}$, $\rho_{lo,39}$, and $\rho_{hi,39}$. Uncertainties in each of these densities were found using:

$$\left(\frac{\sigma_\rho}{\rho}\right)^2 = \left(\frac{\sigma_m}{m}\right)^2 + \left(\frac{\sigma_{Cy}}{C_y}\right)^2 + \left(\frac{\sigma_a}{a}\right)^2 \tag{6}$$

Derived densities that were smaller than their uncertainties were discarded. This sometimes resulted in large gaps in the time series of retained densities, which is not desirable. To correct this, additional derived densities were discarded as necessary to ensure that the time series of retained densities was continuous. For example, if the density at t=-50s exceeded its uncertainty, the densities from t=-49s to t=-40s did not exceed their uncertainties, and the densities from t=-39s to t=+60s exceeded their uncertainties, the derived density at t=-50s was discarded. This completes step 4 (density derivation) of the data processing.

FIGURE - a, sa vs t 1, 7, 39 for P076 FIGURE Cy vs t for 1, 7, 39 for P076 FIGURE rho, srho vs t for 1, 7, 39 for P076 FIGURE ux, uz, phi, theta vs t for P076

Each aerobraking pass has up to six derived density profiles: ρ_{lo}, ρ_{hi}, $\rho_{lo,7}$, $\rho_{hi,7}$, $\rho_{lo,39}$,

and $\rho_{hi,39}$. Each derived density value has an associated altitude. Let z_{max} be the greatest altitude for a given density profile. Values of σ_ρ and $\sigma_{aaero,y}$ at z_{max}, as well as z_{max}, are listed in Table 2 for the three types of high rate density profiles.

Derived densities rely on knowledge of the speed and direction of the spacecraft relative to the atmosphere. The velocity of Odyssey in an inertial frame is determined from SPICE information (Section 3). The velocity of the atmosphere in an inertial frame is determined from the assumption that the atmosphere rotates at the same angular velocity as the solid planet. This assumption is not accurate. Models predict zonal and meridional winds of $\sim$100 ms^{-1} at aerobraking altitudes (REF Bougher papers).

If, instead of assuming solid body rotation for the atmosphere, we assume that there is a zonal wind of 100 ms^{-1}, then derived densities are altered by <1%. A meridional wind of 100 ms^{-1} alters derived densities by $\sim$5%. Data users should be aware of this potential source of error, which is not included in the derived uncertainties (Eqn 6) because wind predictions are so uncertain.

8. Constant Altitude Data Products

The 1-second sampling rate (<1 km vertical resolution) in the derived density profiles is not necessary for many studies of large-scale atmospheric processes. Another dataset of reduced size was generated from ρ_{39} data to support such studies. Orbits for which $\rho_{hi,39}$ data were available used $\rho_{hi,39}$ data. Orbits for which $\rho_{hi,39}$ data were not available used $\rho_{lo,39}$ data.

ρ_{39} measurements for a given orbit were first split in two. All densities before periapsis, including the periapsis density, were assigned to the inbound leg. All densities after periapsis, including the periapsis density, were assigned to the outbound leg. Each leg was

processed separately. Target altitudes were defined as 100 km, 110 km, 120 km, 130 km, 140 km, 150 km, and 160 km. If density measurements existed more than 3 km below the target altitude and more than 3 km above the target altitude, then we proceeded. An exponential fit to all densities within 5 km of the target altitude was then performed. The fitted density scale height and the fitted density at the target altitude were recorded, along with their uncertainties (ref Bevington. Include specific eqns for fitting so that reader can reproduce exactly). Assuming an isothermal atmosphere, temperature, T_ρ, and uncertainty was estimated from the fitted density scale height, H_ρ, using:

$$T_\rho = \frac{\mu g H_\rho}{k_B} \tag{7}$$

where μ is mean molecular mass, assumed to be 43.49 daltons, g is the acceleration due to gravity, and k_B is Boltzmann's constant. The assumed μ, which corresponds to Viking Lander measurements at the surface, is an overestimate (REF Viking, Mars bk, Magalhaes). Light species such as O are more abundant in the thermosphere than near the surface. Data users who wish to make a different assumption concerning μ can simply multiply our T_ρ by the ratio of their desired mean molecular mass to 43.49 daltons. g is given by:

$$g = \frac{GM}{(R_{ref} + z)^2} \tag{8}$$

where R_{ref} is the mean equatorial radius of the MOLA areoid used in this work, 3396 km, G is the gravitational constant, and M is the mass of Mars (REF for MOLA, state and cite value of GM).

No fitted values of ρ, H_ρ, or T_ρ exceeded their uncertainties. One set of results for H_ρ and T_ρ was negative (orbit 12, outbound 130 km, -75 km, s = 29 km, -1340K, 480K). Recall that aerobraking passes are not vertical; they span significant horizontal extent.

Densities do decrease with altitude at 130 km on the outbound leg of this aerobraking pass, presumably due to some kind of wave, so this negative scale height is formally accurate. However, this illustrates that caution should be used when interpreting scale heights derived from non-vertical density profiles. Fitted values of ρ cannot be negative, due to the exponential fitting approach.

The orbits for which constant altitude results were obtained are listed in Table 3. Results were obtained at 110 km and 120 km for almost all orbits, at 100 km for >50% of orbits, and at 140 km outbound for >20% of orbits. Results at 150 km and 160 km are essentially non-existent. The outbound 140 km measurements were obtained at daytime LSTs more frequently than the inbound 140 km measurements, and the difference between daytime and nighttime densities at 140 km explains why there are so many more outbound 140 km measurements than inbound 140 km measurements. Typical uncertainties in fitted ρ, H_ρ, and T_ρ are shown in Table 4.

9. Pressure and Temperature Profiles

Vertical pressure, p, and temperature, T, profiles can be derived from a vertical density profile using:

$$\frac{dp}{dz} = -\rho g \tag{9}$$

$$p = \frac{\rho k_B T}{\mu} \tag{10}$$

where g and μ are as defined in Section 8. Eqn 9 needs an upper boundary condition. If the atmosphere is isothermal, then $p = \rho g H_\rho$, where H_ρ is the density scale height, which can be derived from a fit to the vertical density profile. If applied to aerobraking density profiles, which are non-vertical, this approach will produce biased p and T profiles.

Horizontal gradients in the atmosphere are not properly accounted for. Differences between values of the periapsis pressure derived for the inbound and outbound legs are a particularly visible manifestation of this problem. Nevertheless, we have used this approach to produce p and T profiles corresponding to the inbound and outbound density profiles on each aerobraking pass. $T(p)$ profiles are so much more common in atmospheric modelling than $\rho(z)$ profiles that the production of p and T profiles increases the value of the Odyssey ACC dataset to many potential users despite biases in the p and T profiles.

Pressure and temperature profiles have been derived from the unaveraged densities, from the 7-point averaged densities, and from the 39-point averaged densities. Orbits for which high rate data were available used high rate data. Orbits for which high rate data were not available used low rate data.

The density measurements for a given orbit were first split in two. All densities before periapsis, including the periapsis density, were assigned to the inbound leg. All densities after periapsis, including the periapsis density, were assigned to the outbound leg. Each leg was processed separately. Any measurement whose altitude is greater than the altitude of a density measurement that is less than twice the density uncertainty was discarded. This improves the application of the upper boundary condition for Eqn 9 and the forthcoming Monte Carlo analysis. If the altitude range of the remaining densities was less than 5 km, then no pressure or temperature profile was obtained.

An exponential fit to all densities within 10 km of the altitude of the highest measurement was used to determine the density scale height at the altitude of the highest measurement. Uncertainties in the densities were used to determine the uncertainty in the fitted density scale height (ref Bevington, give equations again).

A Monte Carlo approach was used to obtain the pressure and temperature profiles, with uncertainties. A dummy density profile was generated using the true density profile

and its uncertainties. A dummy density scale height for the top of the profile was generated using the fitted density scale height and its uncertainty. All uncertainties were assumed to correspond to a Gaussian distribution. If any of the dummy density values or the dummy density scale height were negative, then the dummy profiles were generated again. A single pressure profile and a single temperature profile were then obtained using Eqns 9–10. After N pressure/temperature profiles were obtained, the mean and standard deviation pressure/temperature were calculated at each altitude. The uncertainty in pressure/temperature was assumed to equal the standard deviation in the Monte Carlo ensemble. Any p measurement whose altitude is greater than the altitude of a p measurement that is less than its uncertainty was discarded. T measurements were treated similarly.

Periapsis pressure and temperature, and their uncertainties, need special treatment, since they are calculated twice, once for the inbound leg and once for the outbound leg. The best estimate of periapsis conditions are calculated as follows:

$$\frac{1}{\sigma^2_{Xbest}} = \frac{1}{\sigma^2_{Xin}} + \frac{1}{\sigma^2_{Xout}} \tag{11}$$

$$\frac{X_{best}}{\sigma^2_{Xbest}} = \frac{X_{in}}{\sigma^2_{Xin}} + \frac{X_{out}}{\sigma^2_{Xout}} \tag{12}$$

where X is periapsis p or T, X_{in} and X_{out} are the inbound and outbound values of X, σ_{Xin} and σ_{Xout} are their uncertainties, X_{best} is the best estimate of X, and σ_{Xbest} is its uncertainty.

FIGURE - 0.5 (pi-po)/(pi+po) vs orbit number

Acknowledgments

Acknowledgements.

REFERENCES

Spencer, D. A., Blanchard, R. C., Braun, R. D., W., T. S., 1999. Mars Pathfinder entry, descent, and landing reconstruction. J. Spacecraft and Rockets 36 (3), 357–366.

Withers, P., Towner, M. C., Hathi, B., C., Z. J., 2003. Analysis of entry accelerometer data: A case study of Mars Pathfinder. Planet. Space Sci. 51, 541–561.

Table 1. L_s, periapsis latitude, periapsis LST, and beginning and ending periapsis number for the 3:1 – 8:1 resonances

Resonance	L_s (degrees)	Latitude (°N)	LST (hrs)	Beginning Periapsis	Ending Periapsis
3:1	48	45	16	645	656
4:1	57	32	16	710	725
5:1	64	16	15	784	803
6:1	71	−4	15	864	901
7:1	78	−28	15	963	989
8:1	82	−45	15	1030	1057

Table 2. Characteristics of derived high-rate density profiles. Each aerobraking pass has up to six derived density profiles (ρ_{lo}, ρ_{hi}, $\rho_{lo,7}$, $\rho_{hi,7}$, $\rho_{lo,39}$, and $\rho_{hi,39}$). Each derived density value has an associated altitude. Let z_{max} be the greatest altitude for a given density profile. Values of σ_ρ and $\sigma_{aaero,y}$ at z_{max}, as well as z_{max}, are listed here. Periapsis altitude was 110 km at the start of aerobraking, decreased to 95 km by orbit 100, then increased to 115 km at the end of aerobraking.

Type of Average	39-point	7-point	Unaveraged
Start of Aerobraking			
z_{max} (km)	146	145	142
σ_ρ at z_{max} (kg km^{-3})	0.4	0.4	0.6
$\sigma_{aaero,y}$ at z_{max} (m s^{-2})	2×10^{-4}	2×10^{-4}	3×10^{-4}
End of Aerobraking			
z_{max} (km)	134	132	122
σ_ρ at z_{max} (kg km^{-3})	0.6	0.8	4
$\sigma_{aaero,y}$ at z_{max} (m s^{-2})	2×10^{-4}	2×10^{-4}	1.3×10^{-3}

Table 3. Coverage of constant altitude data.

Altitude (km)	Number of orbits	First orbit	Last orbit
Inbound			
100	37	95	146
110	173	46	255
120	316	13	335
130	255	11	336
140	6	7	32
150	0	—	—
160	0	—	—
Outbound			
100	37	95	146
110	173	46	255
120	316	13	335
130	280	11	336
140	77	7	158
150	3	16	29
160	0	—	—

Table 4. Typical uncertainties in constant altitude data

Altitude (km)	σ_ρ (kg km^{-3})	σ_H (km)	σ_T (K)
Outbound			
100	0.176	0.51	9.3
110	0.104	0.33	6.0
120	0.078	0.34	6.1
130	0.083	1.32	23.7
140	0.089	3.01	53.9
150	0.095	5.07	90.4
160	—	—	—
Inbound			
100	0.155	0.14	2.5
110	0.100	0.18	3.3
120	0.076	0.28	5.1
130	0.084	1.36	24.5
140	0.083	2.00	35.9
150	—	—	—
160	—	—	—

Figure Captions

Fig. 1: Atmospheric temperature profile derived by Mars Pathfinder, shown in the black line as a function of altitude. A $\pm 1\sigma$ uncertainty envelope, most significant at high altitudes, is plotted in grey. These data are taken from the PDS archive.

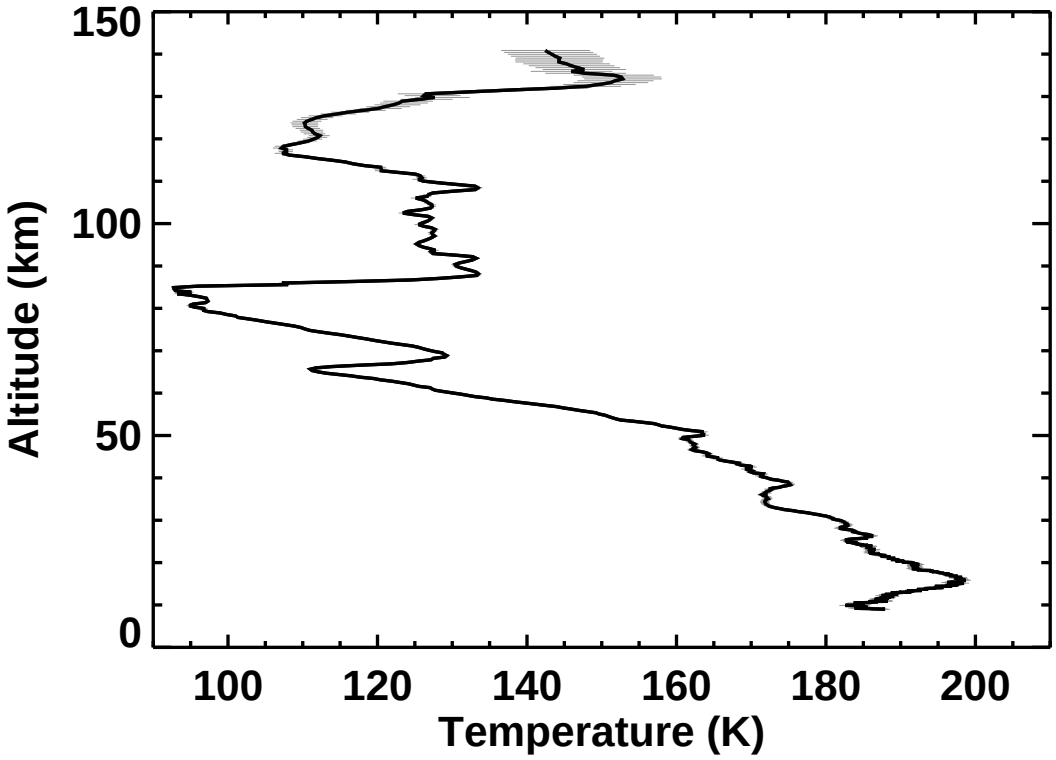

Fig. 1.— Author Paul Withers — Mars Pathfinder Entry Profile